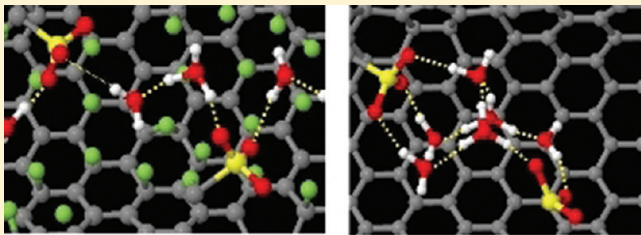


# Ab Initio Simulations of the Effects of Nanoscale Confinement on Proton Transfer in Hydrophobic Environments

Bradley F. Habenicht and Stephen J. Paddison\*

Department of Chemical & Biomolecular Engineering, University of Tennessee, Knoxville, Tennessee 37996, United States

**ABSTRACT:** Carbon nanotubes (CNTs) were functionalized with  $-CF_2SO_3H$  groups and hydrated with 1–3 water molecules per sulfonic acid group to investigate proton dissociation and transport in confined, hydrophobic environments. The distance between sulfonate groups was systematically varied from 6 to 8 Å, and three different CNTs were used to determine the effects of nanoscale confinement. The inner walls of the CNT were either functionalized with fluorine atoms to provide a localized negative charge or left bare to provide a more delocalized charge distribution. The use of ab initio molecular dynamics permitted the study of sulfonate solvation, proton dissociation, and the formation of a hydrogen bonding network without a priori assumptions. It was shown that decreasing the distance between sulfonate groups increased proton dissociation, as well as the interactions between water molecules. As the sulfonate distance increased, connectivity among the water molecules decreased as they formed more isolated clusters around the sulfonate groups. The sulfonate distance and geometry were the most dominant factors in proton dissociation; however, the hydrophobic environment and nanoscale confinement became more important as the distance between sulfonate groups increased.



## INTRODUCTION

Proton transfer in aqueous environments has long been an area of intense study. From the earliest insights of von Grotthuss<sup>1</sup> to state-of-the-art experimental<sup>2–5</sup> and theoretical<sup>6–9</sup> investigations today, proton transfer remains at the forefront of biological, chemical, energy, and materials research. Although the mechanism of proton transport and its curiously high transport in bulk water have been elucidated by experimental<sup>10</sup> and theoretical<sup>11–14</sup> studies, proton transport remains an active area of study. The focus, however, has shifted from bulk solutions to aqueous, protonic systems restricted in size to a few nanometers and subject to hydrophobic environments.<sup>8</sup>

Theoretical<sup>8,15</sup> and experimental<sup>16</sup> investigations show that water readily wets or fills carbon nanotubes (CNTs), even though these nanostructures are shown to be hydrophobic in bulk water.<sup>17</sup> Molecular dynamics simulations show that water forms a molecular “wire” in ultranarrow CNTs.<sup>18</sup> This water wire can increase the proton conductivity through the CNT by a factor of 40. Recent experimental evidence suggests that changing the polarity of the solvent can induce water to fill a fullerene cavity, which is usually a hydrophobic species.<sup>19</sup> Although water molecules may inhabit these hydrophobic environments, their geometry and hydrogen-bond network are drastically altered. Experimental neutron scattering experiments on water molecules encapsulated in CNTs shows that their coordination number (CN) is approximately 1.86.<sup>20</sup> In bulk water, the CN is approximately 3.8,<sup>12</sup> which implies a fundamentally different structure.

These restricting environments and a small number of water molecules in nanoconfined geometries may significantly alter the mechanism of proton conduction from that of bulk water.<sup>8,21</sup> A proton is not an isolated species in bulk water but is instantly

solvated as a hydrated cation such as  $H_3O^+$ ,  $H_5O_2^+$ ,  $H_9O_4^+$ , and so forth.<sup>12</sup> The protonic charge may diffuse with this larger cation in a Brownian-type mechanism, similar to larger cation species ( $Li^+$ ,  $K^+$ , etc.). However, as all hydrogen nuclei in water are equivalent, the protonic charge may diffuse through the hydrogen bonding network without net motion of the initial proton. This mechanism is known as proton hopping or Grotthuss shuttling.<sup>1,12</sup> The introduction of a hydrophobic species into bulk water has been shown to hinder Grotthuss shuttling by interfering with the hydrogen bonding network.<sup>22</sup> In concentrated solutions of strong acids, the anionic species has also been shown to disrupt Grotthuss shuttling.<sup>23</sup> Recent first principles based simulations of several hydrates of triflic acid (i.e.,  $CF_3SO_3H(H_2O)_n$ ,  $n = 1–3, 5$ ) underscore the importance of an extended hydrogen bonding network to facilitate formation of proton defects and long-range proton transport.<sup>24,25</sup> As mentioned above, proton transport is enhanced in ultranarrow CNTs,<sup>18</sup> which has been attributed to enhanced proton shuttling; however, the ascribed mechanism is significantly different than that determined for bulk water.<sup>21</sup>

As one can see, there is still much to be understood about aqueous proton transport, especially in environments that vary significantly from bulk water. A material that invokes several of the issues discussed previously, nanoconfinement, hydrophobic environment, and solvating anions, is a proton exchange membrane (PEM).<sup>5,26</sup> PEMs are used as the separating medium in proton-conducting fuel cells. They serve to facilitate proton

Received: June 20, 2011

Revised: August 9, 2011

Published: August 10, 2011

transport from anode to cathode, provide mechanical and chemical stability, and prevent the permeation of fuel gases. Typical PEMs consist of a hydrophobic polymer backbone, such as poly(tetrafluoroethylene) (PTFE) or poly(ether ketone), that is chemically functionalized with strong acid groups, such as sulfonic acid ( $-\text{SO}_3\text{H}$ ).<sup>26</sup> Low-temperature PEMs require water to transport protons, and upon hydration, these materials phase separate on the nanoscale into hydrophobic domains that contain the polymer backbone and hydrophilic domains that contain water molecules, protons, and the functionalized side chains.<sup>27</sup> The morphology of this phase separation is poorly understood despite intense experimental and theoretical investigations, and several models have been proposed based on the interpretation of experimental data.<sup>26</sup> One of the more recent proposals focuses on Nafion, a perfluorosulfonic acid (PFSA) ionomer that has been extensively studied and posits that at a hydration of 20 vol % ( $\lambda = [\text{H}_2\text{O}]/[\text{SO}_3\text{H}] = 15$ ) the hydrophilic phase forms parallel cylindrical channels with a diameter of 18–35 Å.<sup>28</sup> However, in light of the previous experimental work,<sup>26</sup> it seems unlikely that the morphology is that simple or homogeneous. The interpretation of IR spectroscopy suggests that up to 25% of the OH groups in the hydrophilic phase are exposed to the hydrophobic phase and cannot participate in hydrogen bonding with other water molecules.<sup>29,30</sup> Furthermore, the mechanical manipulation of Nafion membranes has been shown to directly alter small-angle X-ray scattering patterns.<sup>26</sup>

As PFSA ionomers undergo nanoscale phase separation, it has proven difficult to model these systems computationally. Classical molecular dynamics simulations generally incorporate several thousand atoms and have corresponding simulation box lengths that approach 100 Å.<sup>31–33</sup> However, this length is only large enough to include a couple of hydrophilic “pores”, and the ionomer is represented by extremely short polymer units to avoid the intractable task of fully equilibrating the polymer. Researchers have recently employed methods such as large-scale molecular dynamics (MD) with predefined ionomer geometry<sup>34</sup> and building a single, very long, ionomer into a simulation box,<sup>35</sup> but the success of these simulations is not entirely clear. More coarse-grained simulations such as Lennard–Jones MD, where some atomic features are replaced by united atoms,<sup>36</sup> and dissipative particle dynamics,<sup>37–40</sup> where large groups of atoms are replaced by parametrized “beads”, have been used to investigate the relationship between the ionomer characteristic and the phase separated morphology. These methods have shown some success; however, coarse graining of the systems washes out the atomic scale resolution and is likely only valid at higher levels of hydration ( $\lambda > 6$ , at least).

A different approach to computational simulations of PEMs involves using higher level density functional theory to probe the solvation of the pendant side chains and investigate proton transport. These electronic structure calculations and ab initio molecular dynamics (AIMD) simulations are restricted to small systems consisting of only a few hundred atoms but do not require the parametrized potentials utilized by classical MD and coarse grained methods.<sup>41</sup> Electronic structure calculations have been used to probe the pendant side chain's acidity, the effects of sulfonic acid group density, connectivity of the acidic groups, and the hydration of the dissociated proton.<sup>42–45</sup> The authors found that a hydration level of  $\lambda = 3$  was required to promote proton dissociation in isolated protogenic groups, but that association between neighboring acidic groups, or the conjugate bases, enhanced dissociation.<sup>46</sup> It was also shown that ionomer backbone

**Table 1.** Properties of CNT–CF<sub>2</sub>SO<sub>3</sub>H Systems

CNT chirality	diameter (Å)	SS 6 Å	SS 7 Å	SS 8 Å
(14,0)	11.2	5.8	6.7	7.8
(16,0)	13.2	5.6	6.8	8.6
(17,0)	14.1	6.2	6.7	7.7

configurations which increased the interactions of the acidic groups were energetically feasible. AIMD simulations of a model Nafion pore have also been undertaken with differing levels of hydration.<sup>47</sup> The authors showed that proton shuttling occurs at both low and high levels of hydration, but at low hydration, the hydrogen bond network among the water molecules is insufficient to promote net proton transport.<sup>47</sup> Although this AIMD study proved insightful, the ionomer morphology is unlikely to be representative of the real system.

Our previous AIMD simulations into proton dynamics in confined, hydrophobic environments were motivated by the goal to examine proton transport in PFSA systems with a known and regular structure.<sup>48,49</sup> The systems consist of CNTs that are functionalized with –CF<sub>2</sub>SO<sub>3</sub>H groups, that is, the terminal groups of the PFSA ionomers, and water molecules were added to the CNTs. The inner walls of the CNT provided the hydrophobic surface, and the bare CNT walls were contrasted with CNT walls that were fluorinated. Three different diameter CNTs were chosen to investigate the effects of nanoscale confinement, and the sulfonic acid groups were placed at different distances in all three CNTs. The AIMD trajectories showed that the higher sulfonate density increased the proton dissociation but also increased trap states that hinder long-range proton transport.<sup>49</sup> Upon comparing the fluorinated CNTs to those with bare walls, it was found that the fluorine atoms provided a fixed negative charge that was capable of weakly accepting hydrogen bonds from water molecules. This localized negative charge resulted in a stronger hydrogen-bond network that increased dissociation of the acidic proton and weakened the interactions between the water molecules and the sulfonate anions.<sup>48</sup>

In light of the previous results, we have broadened our simulations by systematically varying the distance between sulfonic acid groups from 6 to 8 Å in all three of the chosen CNT systems. We again hydrated the systems to  $\lambda = 1$  and 3 and generated AIMD trajectories for nine fluorinated and nine nonfluorinated CNT systems. This resulted in a total of 36 simulation cells and over 1000 ps of AIMD trajectory. We note that these are model systems, undertaken not to represent an actual channel in a PFSA membrane (channels do not seem to exist in these membranes at such low levels of hydration), but to investigate the impact of acidic group density and geometry, as well as the effects of nanoconfinement and hydrophobic surfaces on proton transport. We also note that a comparison with experimental data is difficult, but we shall attempt to reference the literature whenever possible.

## SIMULATION DETAILS

The (14,0), (16,0), and (17,0) CNTs were chosen to encapsulate the water molecules and –CF<sub>2</sub>SO<sub>3</sub>H groups in the current study.<sup>50</sup> Representative images of the CNTs are shown in Figure 1, and important properties of the systems are detailed in Table 1. It was attempted to place the –CF<sub>2</sub>SO<sub>3</sub>H at regular intervals with spacing of 6, 7, or 8 Å; however, the fixed CNT

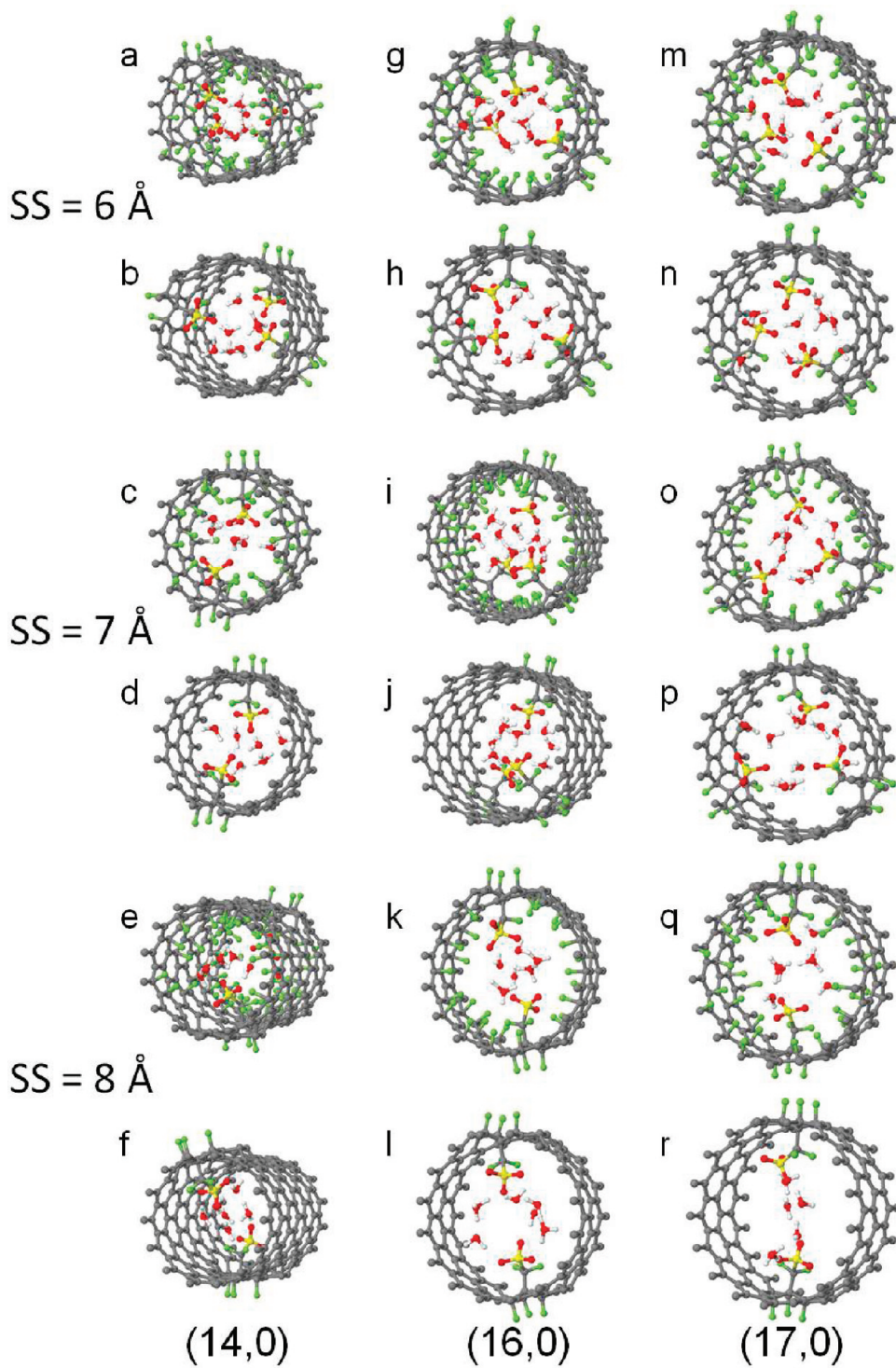


**Figure 1.** CNT– $\text{CF}_2\text{SO}_3\text{H}/\text{H}_2\text{O}$  systems used in this work. Periodic boundary conditions are imposed along the length of the CNT. All CNTs are shown at a hydration of  $\lambda = 3$ . Carbon, fluorine, hydrogen, oxygen, and sulfur atoms are depicted as gray, green, white, red, and yellow spheres, respectively. This color scheme is used throughout this manuscript.

diameter and hexagonal nature of the CNT structure made it difficult to ensure exact spacing of the groups. It has been estimated experimentally that the average sulfur–sulfur (SS) distance in a typical Nafion membrane is about 8 Å.<sup>5</sup> Varying the SS distances is also expected to have a significant effect on proton dissociation and binding energies of the water molecules.<sup>51</sup> Average SS distances are given in Table 1. After the  $-\text{CF}_2\text{SO}_3\text{H}$

had been placed, fluorine atoms were added to the outside of the CNT on the three carbon atoms that were neighbors to the carbon atom attached to the  $-\text{CF}_2\text{SO}_3\text{H}$  group to ensure the acidity of the sulfonate groups were essentially the same. At this point fluorine atoms were attached to the inner walls of the fluorinated CNTs. In the data analysis, we have used “F” to designate the fluorinated systems and “NF” to denote the

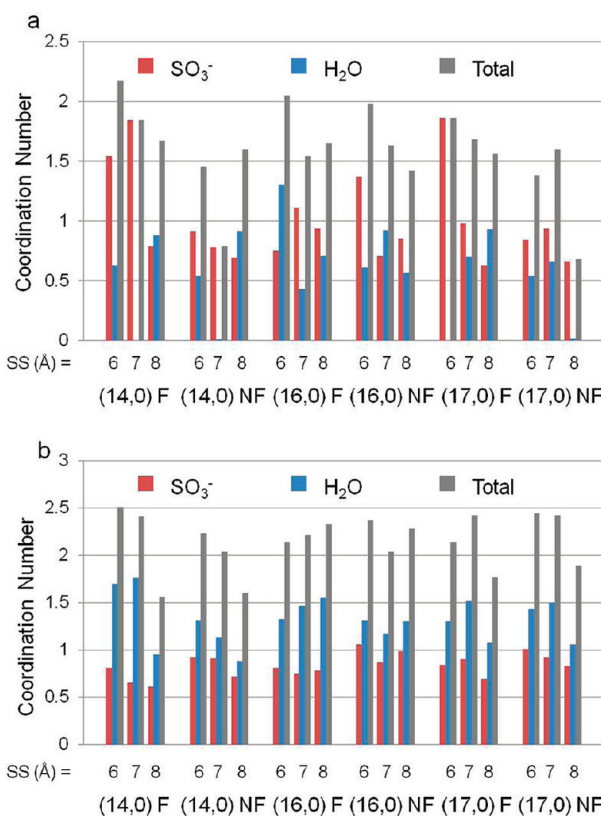


**Figure 2.** Coordination number graphs. CN values represent the average number of hydrogen bonds donated and received by water molecules. The hydration level  $\lambda = 1$  is shown (a), and  $\lambda = 3$  is shown (b).

nonfluorinated. Care was taken to avoid fluorinating neighboring carbon atoms and to provide as homogeneous a distribution as possible without placing fluorine atoms too close to the sulfonate groups. The walls of the CNT and all fluorine atoms were then frozen for the AIMD trajectory. This was for two reasons. First, low energy acoustic modes are active in the CNT at room temperature,<sup>50</sup> and these motions of the cylinder impacted the AIMD results. Second, the fluorine atoms attached to the CNT inner walls were not stable, which it is assumed is due to the curvature of the CNT. The  $-\text{CF}_2\text{SO}_3\text{H}$  groups were allowed to move freely, though little rotation was observed after the initial equilibration. Periodic boundary conditions were imposed along the length of the CNT, and 6 Å of vacuum was added in the perpendicular directions to avoid interactions with other images in the supercell.

The CNT– $\text{CF}_2\text{SO}_3\text{H}$  systems were initially relaxed to their minimum energy configurations, annealed to 600 K via repeated velocity rescaling, and returned to 300 K. After annealing, 3 ps of canonical MD and 3 ps of microcanonical MD were generated to ensure system equilibration. The equilibration trajectory was discarded, and 25–30 ps of Born–Oppenheimer AIMD trajectory was generated in the microcanonical ensemble for data analysis. The time step used was 0.5 fs. All AIMD calculations were generated using the Vienna Ab Initio Simulations (VASP) software package.<sup>52,53</sup> Core electrons were represented using projector-augmented-wave pseudopotentials,<sup>54,55</sup> and the Perdew–Burke–Ernzerhof exchange-correlation functional was utilized.<sup>56</sup> The electronic subsystem was sampled at the  $\Gamma$ -point of the first

**Table 2. Coordination Number Data**

CNT system	$\lambda$	CN $\text{H}_2\text{O}-\text{H}_2\text{O}$			CN $\text{H}_2\text{O}-\text{SO}_3^-$			total CN		
		SS 6 Å	7 Å	8 Å	6 Å	7 Å	8 Å	6 Å	7 Å	8 Å
(14,0) F	1	0.63	0	0.88	1.54	1.84	0.79	2.17	1.84	1.67
(14,0) NF	1	0.54	0.01	0.91	0.91	0.78	0.69	1.45	0.79	1.60
(16,0) F	1	1.30	0.43	0.71	0.75	1.11	0.94	2.05	1.54	1.65
(16,0) NF	1	0.61	0.92	0.57	1.37	0.71	0.85	1.98	1.63	1.42
(17,0) F	1	0	0.70	0.93	1.86	0.98	0.63	1.86	1.68	1.56
(17,0) NF	1	0.54	0.66	0.02	0.84	0.94	0.66	1.38	1.60	0.68
(14,0) F	3	1.70	1.76	0.95	0.81	0.65	0.61	2.51	2.41	1.56
(14,0) NF	3	1.31	1.13	0.88	0.92	0.91	0.72	2.23	2.04	1.60
(16,0) F	3	1.33	1.46	1.55	0.81	0.75	0.78	2.14	2.21	2.33
(16,0) NF	3	1.31	1.17	1.30	1.06	0.87	0.98	2.37	2.04	2.28
(17,0) F	3	1.30	1.52	1.08	0.84	0.90	0.69	2.14	2.42	1.77
(17,0) NF	3	1.43	1.50	1.06	1.01	0.92	0.83	2.44	2.42	1.89

Brillouin zone with a planewave cutoff of 400 eV. All AIMD calculations were done on the Kraken supercomputer, which is based on a Cray XT5 architecture and provides excellent scaling for the VASP software package.<sup>57,58</sup>

## RESULTS AND DISCUSSION

Many of the subsequent results were determined by defining a hydrogen bond network among the water molecules. A hydrogen bond was defined as an oxygen–oxygen distance of less than 3.25 Å and an angle OHO of less than 30°.<sup>7,11</sup> The resulting hydrogen bond network was used to determine the coordination number (CN), or number of nearest neighbors, as well as the connectivity data. The hydrogen bonding of the water molecules was determined in a similar manner and required an oxygen–fluorine distance of less than 3.25 Å and an angle OHF of less than 30°. Although the definition of a hydrogen bond varies in the literature,<sup>59</sup> slightly relaxing or restricting these criteria did not significantly change the results. The authors would also like to note that our systems have relatively few water molecules (only 9 in several of the  $\lambda = 3$  systems) and we were unable to obtain statistically converged dynamical properties, such as diffusion coefficients and hydrogen bond autocorrelation functions.

**Coordination Numbers (CNs).** The CN data are the average number of donated and accepted hydrogen bonds for each water molecule and are presented in Figure 2 and Table 2. Figure 2a shows the CNs at a hydration of  $\lambda = 1$ , and Figure 2b shows the CNs at  $\lambda = 3$ . As one can see, there are no clear trends in the hydrogen bonding of the water molecules at  $\lambda = 1$ . The interactions are dominated by the sulfonate geometry, and in some cases, the water molecules are completely isolated from one another. The average number of neighbors is generally around 1.5, and it is clear that a strong hydrogen bond network does not form at this low hydration. The CNs are generally greater when the SS distance is smaller, which is due to a single water molecule being able to interact with more than one sulfonate group. At a SS distance of 8 Å, a single water molecule cannot bridge two sulfonate groups, and the CN decreases.<sup>49</sup>

When the hydration level is increased to  $\lambda = 3$ , the water molecules cluster together and interact more among themselves, and the sulfonate groups and the CNs increase. However, the CN is still significantly lower than that of bulk water. In the nonfluorinated systems the water molecules have a greater

interaction with the sulfonate groups when compared to the fluorinated systems, as can be seen in Figure 2b. The fluorinated environment seems to stabilize interactions among water molecules, and thus, the water molecules are not bound as strongly to the sulfonate groups as they are in the nonfluorinated systems. A general trend is that the CNs decrease as the sulfonate groups are moved further apart, although this does not hold true in all of the systems, which is a further indication that the sulfonate geometry dictates the nature of the hydrogen bond network. One also notes that the CNs are similar for all three CNTs. This indicates that the geometry of the sulfonate groups is more important to the hydrogen bonding network than is nanoscale confinement. It also indicates that the water molecules are bound to the sulfonate groups, as opposed to clustering among themselves in the larger CNT systems.

**Connectivity.** To further analyze the hydrogen-bond network in the CNT systems, we have employed a recursive branching algorithm to determine the connectivity of the water molecules. Details are available in our previous publication,<sup>49</sup> however, the general notion is to determine the number of independent water clusters and count the average number of sulfonate oxygen atoms and water molecules within those clusters. A cluster was required to have at least three members hydrogen bonding to be counted.

**Table 3. Connectivity Data and Average Number of Chains**

CNT system	$\lambda$	average number of chains		
		SS 6 Å	7 Å	8 Å
(14,0) F	1	1.48	0.81	0.87
(14,0) NF	1	0.74	0.32	0.88
(16,0) F	1	1.26	1.52	0.46
(16,0) NF	1	0.99	0.92	0.51
(17,0) F	1	0.12	0.91	0.67
(17,0) NF	1	1.03	0.88	0.05
(14,0) F	3	1.99	1.48	1.95
(14,0) NF	3	2.18	1.55	1.97
(16,0) F	3	2.03	2.47	1.54
(16,0) NF	3	2.47	2.69	1.75
(17,0) F	3	2.19	1.92	1.84
(17,0) NF	3	2.17	2.44	1.71

**Table 4. Connectivity Data and Average Length of Chains**

CNT system	$\lambda$	average number of H <sub>2</sub> O oxygen atoms			average number of SO <sub>3</sub> <sup>-</sup> oxygen atoms		
		SS 6 Å	7 Å	8 Å	6 Å	7 Å	8 Å
(14,0) F	1	1.59	2.00	2.00	1.73	1.00	1.58
(14,0) NF	1	1.85	1.97	2.00	1.16	1.19	1.42
(16,0) F	1	2.67	1.46	1.94	1.46	1.8	1.06
(16,0) NF	1	1.67	1.68	1.6	1.88	1.35	1.45
(17,0) F	1	1.24	1.85	1.98	2.11	1.33	1.03
(17,0) NF	1	1.53	2.22	1.17	1.94	1.05	2.02
(14,0) F	3	4.41	4.42	2.46	1.16	0.89	2.07
(14,0) NF	3	3.34	3.36	2.26	1.52	1.67	1.85
(16,0) F	3	3.99	3.29	3.19	2.07	1.19	1.10
(16,0) NF	3	3.43	2.88	2.99	1.93	1.59	1.62
(17,0) F	3	3.66	3.73	2.57	1.76	1.57	1.63
(17,0) NF	3	3.95	3.29	2.74	1.8	1.84	1.86

The results of this analysis are presented in Tables 3 and 4 and depicted in Figures 3 and 4.

Figure 3a depicts the hydrogen bond connectivity at  $\lambda = 1$ . Because of the small number of water molecules in the CNT systems, most counted clusters only have three members. In the (16,0) and (17,0) CNT systems the contributions from water molecules and sulfonate groups are mixed, and there are longer chains on average when the SS is smaller. In the (14,0) systems, the average number of oxygen atoms in the chains is more irregular due to the more confined geometry of these systems.

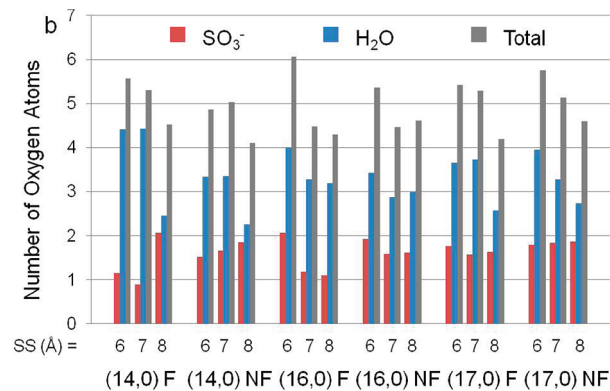
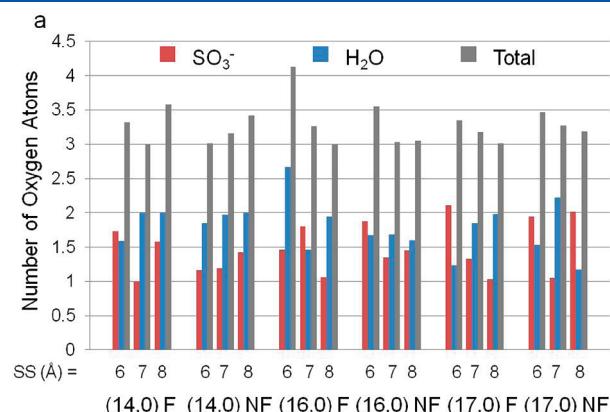


**Figure 3.** Connectivity graphs for the current systems. Graphs depict the average number and type of oxygen atoms in the hydrogen-bonded chain. The hydration level  $\lambda = 1$  is shown (a), and  $\lambda = 3$  is shown (b).

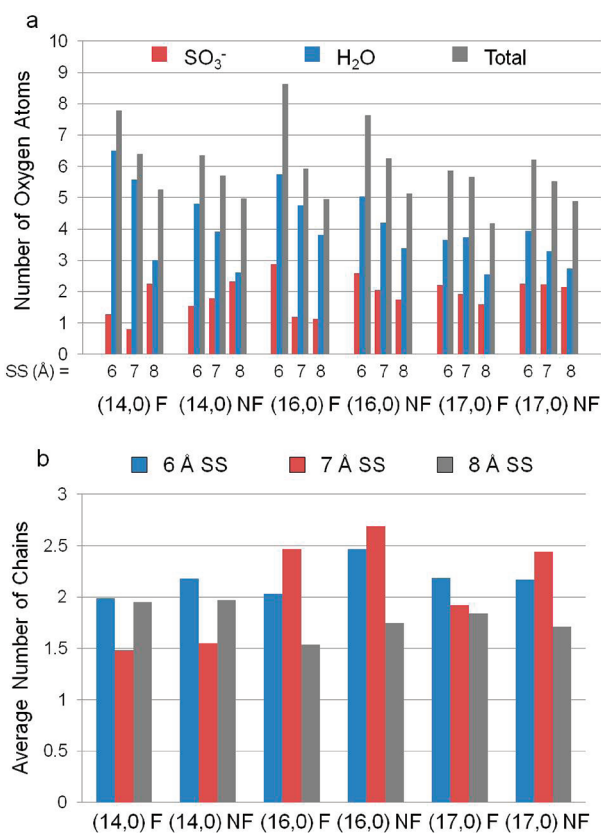


**Figure 4.** Connectivity data for the longest chain in a simulation cell at a hydration of  $\lambda = 3$  (a) and the average number of chains per simulation cell at a hydration of  $\lambda = 3$  (b).

Still, the connectivity data are similar in both the fluorinated and the nonfluorinated systems, which indicates the importance of the sulfonate geometry compared to nanoconfinement and hydrophobic environment. Once the hydration is increased to  $\lambda = 3$ , there is an increased contribution from the additional water molecules, and the average number of oxygen atoms in the clusters increases to between 4 and 6. The average number of water molecules in the chains decreases as the SS distance increases, which suggests a greater clustering among isolated sulfonate groups, as opposed to uniform solvation. In other words, the water molecules are still bound to the sulfonate groups instead of forming clusters on their own. This is further illustrated by the fact that on average, most of the systems have less than two sulfonate oxygen atom in the chains.

The number of oxygen atoms on average in the longest chain at a hydration of  $\lambda = 3$  is depicted in Figure 4a, while the average number of chains at  $\lambda = 3$  is shown in part b. The clusters or chains of water molecules tend to decrease in size as the SS distance is increased. Since the average number of chains does not vary greatly, as shown in Figure 4b, this indicates a decrease in the ordering of the hydrogen-bond network and more water molecules clustering around the sulfonate groups, but not participating larger clusters. In the (16,0) and (17,0) systems, the average number of chains decreases as the SS distance increases, which is attributed to an increase in the free volume of the system. The increase of free volume decreases the strength of the hydrogen bond network and increases the number of water molecules clustered

**Table 5. H–F Data**

CNT system	$\lambda$	percent time H–F bond exists		
		SS 6 Å	7 Å	8 Å
(14,0) F	1	3.40	40.79	44.43
(16,0) F	1	7.22	41.95	13.12
(17,0) F	1	64.90	4.61	2.94
(14,0) F	3	25.60	15.05	44.48
(16,0) F	3	31.06	20.43	25.78
(17,0) F	3	29.11	13.82	20.12

around the sulfonate groups. The trend is not observed in the (14,0) systems, which is due to the nanoscale confinement in this smaller CNT.

**H–F Hydrogen Bonding.** As mentioned above, we have used the same parameters to define a hydrogen bond between two water molecules and a fluorine atom accepting a hydrogen bond from a water molecule (H–F bond). The results of this analysis are presented in Table 5, and it should be noted that an H–F bond was required to exist for 5 fs to be counted. In our previous publication, we noted that the  $-\text{CF}_2$  groups are able to accept hydrogen bonds, but that it is fairly rare in the nonfluorinated CNT systems and only hydrogen bonding to fluorine atoms on the CNT walls is presented in Table 5. From the data in Table 5, one can see that interactions between water molecules and fluorine atoms are a fairly regular feature of these AIMD simulations. IR spectroscopy has been used to estimate that up to 25% of the possible  $\text{H}_2\text{O}$  hydrogen bonds are not saturated in a hydrated Nafion membrane and that these OH groups are exposed to the PTFE phase.<sup>29,30</sup> At a hydration of  $\lambda = 1$ , the values are scattered with some of the sulfonate geometries encouraging interactions with the fluorine atoms and other sulfonate geometries shielding the water molecules from the fluorine atoms. As the hydration level is increased to  $\lambda = 3$ , the values become more uniform and range from 13–45% of the time an H–F bond is present. These values also indicate that the H–F bonding is fairly weak and transient, especially compared to hydrogen bonding among water molecules and sulfonate groups.

**Dissociation.** Under the conditions of minimal hydration undertaken in the present study, the acidic protons are not always completely dissociated from the sulfonate anions. To quantify the proton dissociation, we have defined three distinct states: bound, shared, and dissociated. A proton is said to be bound if it is within 1.35 Å of an oxygen atom that is part of a sulfonate group and there is no oxygen atom of a water molecule within 1.35 Å. A proton is in the shared state if it is within 1.35 Å of a sulfonate oxygen atom and there is an oxygen atom from a water molecule within 1.35 Å. A proton is considered dissociated if there is not a sulfonate oxygen atom within 1.35 Å. Previous electronic structure calculations have shown that the protons begin to dissociate from the sulfonate anions at a hydration of  $\lambda = 3$ , although interactions between neighboring sulfonic acid groups can enhance the dissociation.<sup>45</sup> The present study is at 300 K, and thermal effects are expected to increase proton dissociation, although simulations predict that entropic effects decrease proton dissociation at low levels of hydration.<sup>60</sup> Sulfonate geometry and the nature of the hydrophobic environment are also expected to influence proton dissociation.<sup>48</sup> The results of the dissociation analysis are presented in Table 6.

**Table 6. Dissociation Data**

CNT system	$\lambda$	SS	bound			shared			dissociated		
			6 Å	7 Å	8 Å	6 Å	7 Å	8 Å	6 Å	7 Å	8 Å
(14,0) F	1	45.5	12.3	46.8	26.1	69.2	5	28.4	18.52	48.2	
(14,0) NF	1	55.3	96.4	89.5	19.6	3.6	10.3	25.1	0.1	0.2	
(16,0) F	1	63.8	47.2	91.4	2.3	43.1	8.5	33.9	9.7	0.1	
(16,0) NF	1	32.5	78.9	96.9	28.0	9.6	3.1	39.5	11.5	0	
(17,0) F	1	12.5	73.8	54.2	60.6	19.1	27.2	26.9	7.1	18.6	
(17,0) NF	1	59.2	75.6	99.4	17.3	24.2	0.6	23.5	0.16	0	
(14,0) F	3	0.04	0.05	0.1	3.06	0.95	9.0	96.9	99.0	90.9	
(14,0) NF	3	0.04	0.04	20.1	9.5	12.1	26.3	90.5	87.9	53.6	
(16,0) F	3	0	0	1.3	9.6	11.6	14.3	90.4	88.4	84.4	
(16,0) NF	3	0.1	9.7	6.9	1.6	9.6	22.4	98.3	80.7	70.7	
(17,0) F	3	1.2	1.3	7.3	9.5	17.0	21.3	89.3	81.7	71.4	
(17,0) NF	3	0	1.4	1.3	8.9	23.5	14.1	91.1	75.1	84.6	

The proton dissociation data at a hydration of  $\lambda = 1$  shows the importance of sulfonate interactions on proton dissociation. When the average SS distance is only 6 Å, a proton is dissociated 20–40% of the AIMD trajectory. When the SS distance increases to 7 Å, the percent dissociation drops to below 20% for all of the systems, and two of the nonfluorinated systems do not see any proton dissociation. This trend is generally followed at an SS distance of 8 Å where the percent dissociation in the nonfluorinated systems and the (16,0) fluorinated system drops to almost zero. The exceptions to this are the fluorinated (14,0) and (17,0) systems. In these two systems, an acidic proton on one of the sulfonate groups interacts strongly with a nearby fluorine atom on the CNT wall, as seen in Figure 5. The water molecules are unable to solvate one of the acidic protons, which results in two water molecules interacting with a single acidic proton. This nonuniform solvation of the acidic groups, coupled with nearby fluorine atoms that can accept hydrogen bonds and stabilize the dissociated proton, significantly increases proton dissociation when compared to a more uniform solvation. Electronic structure calculations indicate that prior to proton dissociation uniform solvation of the sulfonate groups is energetically favored; however, nonuniform solvation configurations that facilitate proton dissociation are found to be preferred.<sup>43</sup> The proton dissociation data at a hydration of  $\lambda = 1$  illustrate the significant impact of sulfonate geometry on proton dissociation.

Increasing the hydration to  $\lambda = 3$  dramatically increases the proton dissociation in the AIMD simulations. For the smallest sulfonate separation of 6 Å, all of the systems show proton dissociation nearly 90% of the time. As the SS distance increases to 7 Å, the dissociation falls to above 75% of the time, and at an SS distance of 8 Å, 50–90% of the protons are dissociated. In general, the fluorinated systems show slightly more dissociation than the nonfluorinated systems; however, it is clear that the SS distance is more influential in proton dissociation than is the hydrophobic environment.

The nonfluorinated (14,0) system shows a steep drop in proton dissociation at an SS distance of 8 Å, especially compared with the fluorinated (14,0) system. The small confinement of the (14,0) CNT and the larger spacing of the sulfonate groups allows more interaction with the fluorine atoms and/or bare CNT walls than is possible in the larger systems (Figure 6). In the fluorinated system, the fluorine atoms stabilize solvation of the

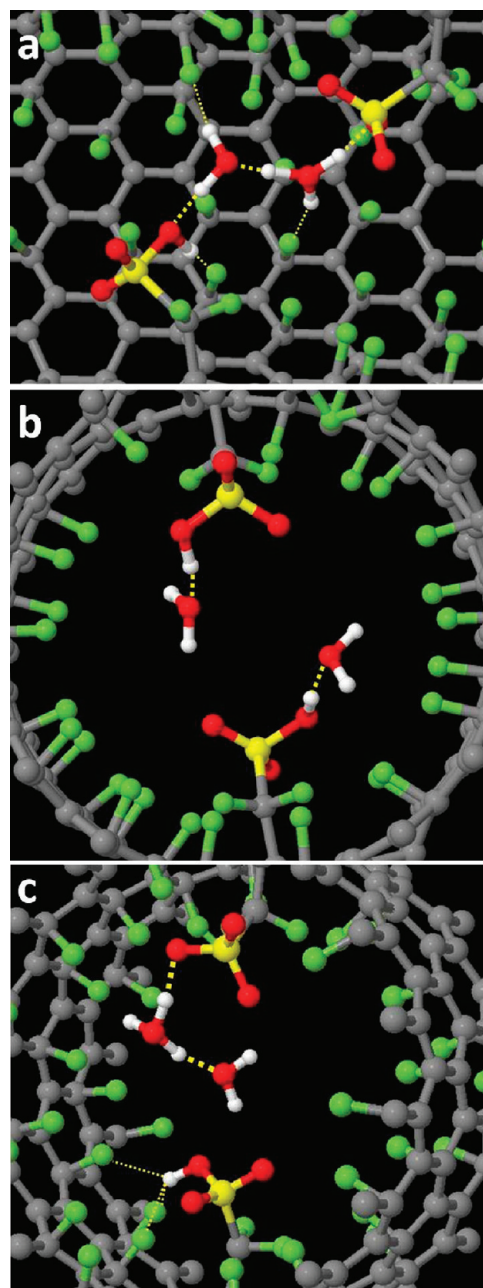


**Figure 5.** Hydrogen-bonding configurations in fluorinated CNT systems at a hydration of  $\lambda = 1$  and an SS distance of 8 Å. The (14,0), (16,0) and (17,0) CNT systems are shown in parts a, b, and c. Thicker yellow lines indicate hydrogen bonding between water molecules and sulfonate oxygen atoms. Thinner yellow lines depict H–F bonding. H–F bonding between a protonated sulfonate group and fluorine atoms bound to the CNT walls is seen in the (14,0) and (17,0) systems (a and c) but is not observed in the (16,0) system (b). Atoms are removed for clarity in part a.

sulfonate groups and a near continuous “wire” of water molecules through the CNT. This is in contrast to the nonfluorinated system where the water molecules form a cluster between the two sulfonate groups. This small cluster contains two dissociated protons that are stabilized as hydronium-like ions ( $\text{H}_3\text{O}^+$ ). The two hydronium ions both donate a hydrogen bond to a single water molecule due to their proximity. Any random motion of

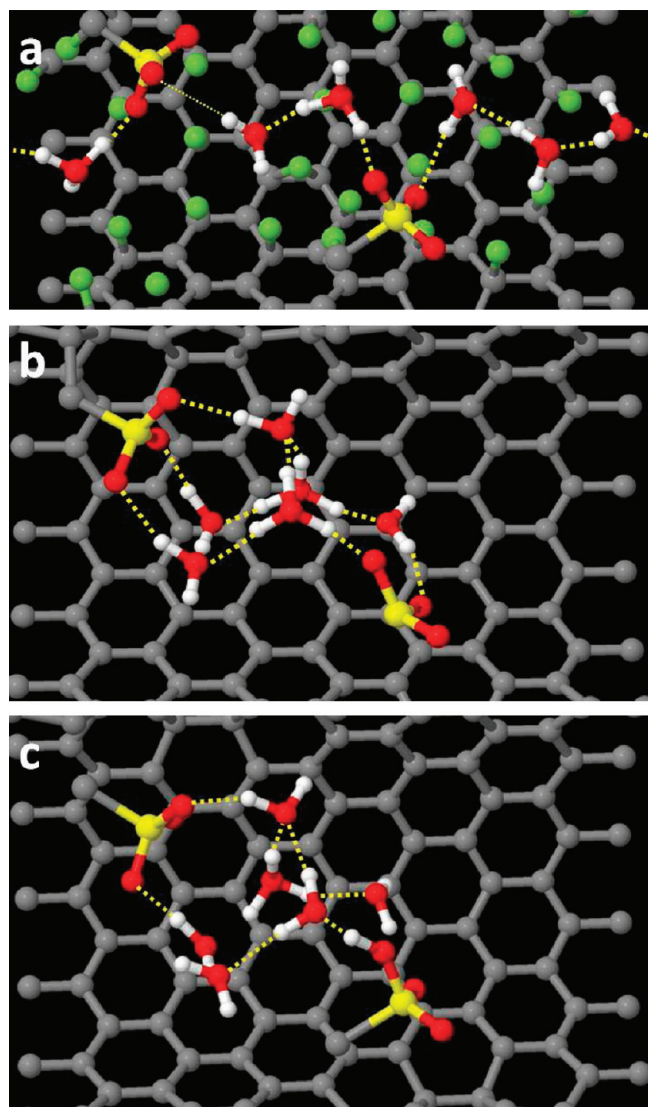


**Figure 6.** Differences in hydrogen-bonding network in the (14,0) systems at a hydration of  $\lambda = 3$  and an SS distance of 8 Å. The (14,0) fluorinated system is shown in part a with a wire-like hydrogen bond network that spans the simulation cell. The (14,0) nonfluorinated system is depicted in part b with a much more clustered hydrogen bond network. Two hydronium ions ( $\text{H}_3\text{O}^+$ ) donate hydrogen bonds to the same water molecule, and any change in its orientation causes the acidic proton to return to the sulfonate group, as shown in part c. Yellow lines denote hydrogen bonds. Atoms were removed from the CNT walls for clarity.

this water molecule that breaks one of these hydrogen bonds strongly disrupts the hydrogen-bond network and causes the proton to return to the sulfonate group, which explains the low percent dissociation observed. This system also underscores the fragility of the hydrogen bonding network at such a low level of hydration. Aside from this case, the (14,0) systems generally have a greater degree of dissociation than their counterparts with larger diameters.

As has been reiterated throughout this manuscript, the geometry and spacing of the sulfonate anions have a very large influence on the dynamics of proton transport in the systems studied. The sulfonate geometry has more influence than the hydrophobic environment or the degree of confinement. Decreasing the

SS distance increases the dissociation of the acidic protons under conditions of minimal hydration. A smaller SS distance also generally increases the CNs of the water molecules and the size and connectivity of the hydrogen-bonded clusters. As the SS distance increases, the water molecules increasingly cluster around the sulfonate groups in smaller chains. The hydrogen bond networks of the water molecules become more isolated as the hydration is not great enough to form hydrogen bonding between the more distant sulfonate groups. Furthermore, the water molecules are more inclined to cluster around the sulfonate groups, as opposed to forming water and proton clusters away from the anionic groups.

The hydrophobic nature of the nanoconfined environment is pronouncedly different with the bare CNT walls and those that have been fluorinated. The bare walls of the CNT have a delocalized charge distribution, while the fluorinated CNT walls provide a fixed negative charge that can accept hydrogen bonds from water molecules or cationic species such as Eigen or Zundel ions. The water molecules do not interact strongly with the fluorine atoms, and the H–F bonding should be considered weak and transient, especially compared to hydrogen bonding among the water molecules and between water molecules and sulfonate anions. However, the bare CNT walls are more repulsive than the fluorinated walls, which is manifest in the greater  $\text{H}_2\text{O}-\text{SO}_3^-$  CNs of the water molecules in the non-fluorinated CNTs. The fluorine atoms' ability to accept hydrogen bonds does strengthen the water hydrogen-bond network and increase proton dissociation, but, as indicated by the similarities in CN, connectivity, and proton dissociation, this strengthening is a weak effect.

The effects of nanoconfinement were primarily manifest in the (14,0) CNT, which has a diameter of 11.2 Å. The (16,0) CNT, which has a diameter of 13.2 Å, did not show nearly as much influence of confinement, even though its diameter is only 2 Å larger than the (14,0). The confinement effects influence the dynamics in two ways. First, greater confinement increases the interactions between the CNT walls and the water molecules and protons. This effect is illustrated best by the (14,0) CNT with an SS distance of 8 Å, as depicted in Figure 6. The fluorinated and nonfluorinated CNT systems have a vastly different hydrogen-bond network, where the fluorinated system supports an extended hydrogen-bond network and the nonfluorinated system has more free volume and a clustering of water molecules and protons between two sulfonate groups. These two different networks are primarily a result of increased interaction with the CNT walls. Second, confinement directly affects the possibly geometries of the sulfonate groups. In the (14,0) CNT with an SS distance of 8 Å, the CNT had to be considerably lengthened to get the sulfonate groups far enough apart. In contrast, in the (16,0) and (17,0) CNTs, the diameter is great enough that the sulfonate groups could be placed across the diameter of the CNT, as in Figures 1 and 5. Thus, a small increase in the diameter of the hydrophilic phase can have a marked impact on the proton transport at very small channel diameters, but as the size of the hydrophilic phase increases, this impact quickly decreases.

## CONCLUSIONS

We have used CNTs functionalized with  $-\text{CF}_2\text{SO}_3\text{H}$  groups to investigate proton dissociation and transport in confined hydrophobic environments under conditions of minimal hydration. In general, the sulfonate distance and geometry had the greatest effect on proton transport and the clustering of the water

molecules. Decreasing the SS distance increased the connectivity of the water molecules and increased proton dissociation. As the SS distance increased, the water molecules tended to form isolated clusters around the sulfonate groups, and nonuniform solvation of the sulfonate groups that increased proton dissociation was the preferred orientation. The fluorinated systems had a stronger hydrogen-bonding network among the water molecules that slightly increased proton dissociation.

The effect of the hydrophobic interface was most pronounced in the (14,0) systems with an SS distance of 8 Å. Because of the small diameter of the (14,0) CNT, the water molecules experienced the greatest exposure to the hydrophobic phase. The fluorine atoms stabilized the water hydrogen bonding network and increased proton dissociation, while bare walls of the nonfluorinated CNT forced the water molecules to cluster together between two sulfonate groups. This small cluster contained two hydronium ions in close proximity, which resulted in a fragile hydrogen bond network. Confinement effects were only pronounced in the (14,0) CNT, even though the (16,0) CNT had a diameter only 2 Å larger. Thus, the effects of nanoconfinement are only significant at small distances and slight increases in the size of the hydrophobic cavity can have pronounced effects on the clustering of water molecules and mechanisms of proton transport.

## AUTHOR INFORMATION

### Corresponding Author

\*E-mail: spaddison@utk.edu.

## ACKNOWLEDGMENT

This work was supported by the U.S. Army Research Laboratory and the U.S. Army Research Office under Contract Number W911NF-07-1-0085. The computations were made feasible through TeraGrid resources provided on the Kraken supercomputer at the National Institute for Computational Sciences, NICS, (<http://www.nics.tennessee.edu>), a University of Tennessee/Oak Ridge National Laboratory facility funded by the National Science Foundation (NSF).

## REFERENCES

- (1) von Grotthuss, C. J. D. *Ann. Chim.* **1806**, 58, 54.
- (2) Garczarek, F.; Gerwert, K. *Nature* **2006**, 439, 109.
- (3) Li, B.; Zhao, J.; Onda, K.; Jordan, K. D.; Yang, J. L.; Petek, H. *Science* **2006**, 311, 1436.
- (4) Tarbuck, T. L.; Ota, S. T.; Richmond, G. L. *J. Am. Chem. Soc.* **2006**, 128, 14519.
- (5) Kreuer, K. D.; Paddison, S. J.; Spohr, E.; Schuster, M. *Chem. Rev.* **2004**, 104, 4637.
- (6) Marx, D. *ChemPhysChem* **2006**, 7, 1848.
- (7) Laage, D.; Hynes, J. T. *Science* **2006**, 311, 832.
- (8) Rasaiah, J. C.; Garde, S.; Hummer, G. *Annu. Rev. Phys. Chem.* **2008**, 59, 713.
- (9) Voth, G. A. *Acc. Chem. Res.* **2006**, 39, 143.
- (10) Vener, M. V.; Librovich, N. B. *Int. Rev. Phys. Chem.* **2009**, 28, 407.
- (11) Marx, D.; Tuckerman, M. E.; Hutter, J.; Parrinello, M. *Nature* **1999**, 397, 601.
- (12) Agmon, N. *Chem. Phys. Lett.* **1995**, 244, 456.
- (13) Lapid, H.; Agmon, N.; Petersen, M. K.; Voth, G. A. *J. Chem. Phys.* **2005**, 122, 014506.
- (14) Markovitch, O.; Chen, H.; Izvekov, S.; Paesani, F.; Voth, G. A.; Agmon, N. *J. Phys. Chem. B* **2008**, 112, 9456.
- (15) Sansom, M. S. P.; Biggin, P. C. *Nature* **2001**, 414, 156.
- (16) Tao, Y. S.; Muramatsu, H.; Endo, M.; Kaneko, K. *J. Am. Chem. Soc.* **2010**, 132, 1214.
- (17) O'Connell, M. J.; Boul, P.; Ericson, L. M.; Huffman, C.; Wang, Y. H.; Haroz, E.; Kuper, C.; Tour, J.; Ausman, K. D.; Smalley, R. E. *Chem. Phys. Lett.* **2001**, 342, 265.
- (18) Dellago, C.; Naor, M. M.; Hummer, G. *Phys. Rev. Lett.* **2003**, 90, 105902.
- (19) Frunzi, M.; Baldwin, A. M.; Shibata, N.; Iwamatsu, S. I.; Lawler, R. G.; Turro, N. J. *J. Phys. Chem. A* **2011**, 115, 735.
- (20) Kolesnikov, A. I.; Zanotti, J. M.; Loong, C. K.; Thiagarajan, P.; Moravsky, A. P.; Louffy, R. O.; Burnham, C. *J. Phys. Rev. Lett.* **2004**, 93, 4.
- (21) Cao, Z.; Peng, Y. X.; Yan, T. Y.; Li, S.; Li, A. L.; Voth, G. A. *J. Am. Chem. Soc.* **2010**, 132, 11395.
- (22) Bonn, M.; Bakker, H. J.; Rago, G.; Pouzy, F.; Siekierzycka, J. R.; Brouwer, A. M.; Bonn, D. *J. Am. Chem. Soc.* **2009**, 131, 17070.
- (23) Choe, Y. K.; Tsuchida, E.; Ikeshoji, T. *J. Chem. Phys.* **2007**, 126, 9.
- (24) Hayes, R. L.; Paddison, S. J.; Tuckerman, M. E. *J. Phys. Chem. B* **2009**, 113, 16574.
- (25) Hayes, R. L.; Paddison, S. J.; Tuckerman, M. E. *J. Phys. Chem. A* **2011**, 115, 6112.
- (26) Mauritz, K. A.; Moore, R. B. *Chem. Rev.* **2004**, 104, 4535.
- (27) Kreuer, K. D. *J. Membr. Sci.* **2001**, 185, 29.
- (28) Schmidt-Rohr, K.; Chen, Q. *Nat. Mater.* **2008**, 7, 75.
- (29) Falk, M. *Can. J. Chem.* **1980**, 58, 1495.
- (30) Moilanen, D. E.; Piletic, I. R.; Fayer, M. D. *J. Phys. Chem. A* **2006**, 110, 9084.
- (31) Vishnyakov, A.; Neimark, A. V. *J. Phys. Chem. B* **2001**, 105, 9586.
- (32) Urata, S.; Irisawa, J.; Takada, A.; Shinoda, W.; Suzuki, S.; Mikami, M. *J. Phys. Chem. B* **2005**, 109, 4269.
- (33) Jang, S. S.; Molinero, V.; Cagin, T.; Goddard, W. A. *Solid State Ionics* **2004**, 175, 805.
- (34) Knox, C. K.; Voth, G. A. *J. Phys. Chem. B* **2010**, 114, 3205.
- (35) Hristov, I. H.; Paddison, S. J.; Paul, R. *J. Phys. Chem. B* **2008**, 112, 2937.
- (36) Malek, K.; Eikerling, M.; Wang, Q. P.; Liu, Z. S.; Otsuka, S.; Akizuki, K.; Abe, M. *J. Chem. Phys.* **2008**, 129, 204702.
- (37) Wu, D.-S.; Paddison, S. J.; Elliott, J. A. *Energy Environ. Sci.* **2008**, 1, 284.
- (38) Wu, D. S.; Paddison, S. J.; Elliott, J. A. *Macromolecules* **2009**, 42, 3358.
- (39) Wu, D. S.; Paddison, S. J.; Elliott, J. A.; Hamrock, S. J. *Langmuir* **2010**, 26, 14308.
- (40) Elliott, J. A.; Wu, D.; Paddison, S. J.; Moore, R. B. *Soft Matter* **2011**, 7, 6729.
- (41) Tuckerman, M. E. *J. Phys.: Condens. Matter* **2002**, 14, R1297.
- (42) Paddison, S. J. Proton Conduction in PEMs: Complexity, Cooperativity and Connectivity. In *Device and Materials Modeling in PEM Fuel Cells*; Springer-Verlag Berlin: Berlin, 2008; Vol. 113, pp 385.
- (43) Paddison, S. J.; Elliott, J. A. *Solid State Ionics* **2007**, 178, 561.
- (44) Paddison, S. J.; Elliott, J. A. *Solid State Ionics* **2006**, 177, 2385.
- (45) Paddison, S. J.; Elliott, J. A. *J. Phys. Chem. A* **2005**, 109, 7583.
- (46) Paddison, S. J.; Elliott, J. A. *Phys. Chem. Chem. Phys.* **2006**, 8, 2193.
- (47) Choe, Y. K.; Tsuchida, E.; Ikeshoji, T.; Yamakawa, S.; Hyodo, S. *Phys. Chem. Chem. Phys.* **2009**, 11, 3892.
- (48) Habenicht, B. F.; Paddison, S. J.; Tuckerman, M. E. *Phys. Chem. Chem. Phys.* **2010**, 12, 8728.
- (49) Habenicht, B. F.; Paddison, S. J.; Tuckerman, M. E. *J. Mater. Chem.* **2010**, 20, 6342.
- (50) Saito, R.; Dresselhaus, G.; Dresselhaus, M. S. *Physical Properties of Carbon Nanotubes*; World Scientific Publishing Company: River Edge, NJ, 1998.
- (51) Roudgar, A.; Narasimachary, S. P.; Eikerling, M. *J. Phys. Chem. B* **2006**, 110, 20469.
- (52) Kresse, G.; Furthmuller, J. *Comput. Mater. Sci.* **1996**, 6, 15.

- (53) Kresse, G.; Furthmuller, J. *Phys. Rev. B* **1996**, *54*, 11169.  
(54) Blochl, P. E. *Phys. Rev. B* **1994**, *50*, 17953.  
(55) Kresse, G.; Joubert, D. *Phys. Rev. B* **1999**, *59*, 1758.  
(56) Perdew, J. P.; Burke, K.; Ernzerhof, M. *Phys. Rev. Lett.* **1996**, *77*, 3865.  
(57) NICS Homepage. <http://www.nics.tennessee.edu>.  
(58) Kent, P. R. C. *J. Phys.: Conf. Ser.* **2008**, 012058.  
(59) Petersen, M. K.; Hatt, A. J.; Voth, G. A. *J. Phys. Chem. B* **2008**, *112*, 7754.  
(60) Glezakou, V.-A.; Dupuis, M.; Mundy, C. *J. Phys. Chem. Chem. Phys.* **2007**, *9*, 5752.